Supplement of The Cryosphere, 20, 1589–1598, 2026
https://doi.org/10.5194/tc-20-1589-2026-supplement

The Cryosphere Open Access EGU

Supplement of

Brief communication: Updated grounding line mapping in the Amundsen Sea Embayment, Antarctica, from one day repeat Sentinel-1 SAR data

Jonas K. Andersen et al.

Correspondence to: Jonas K. Andersen (joka@ign.ku.dk)

Supplementary sections

Section S1 - Estimating tide- and pressure-induced sea surface height difference

Supplementary Tables

Table S1 - Acquisition dates for Sentinel-1 images used in double-difference interferograms along with estimated sea surface height

Supplementary Figures

Figure S1 - Coverage of Sentinel-1 1-day repeat imagery

Figure S2 - Examples of short-term variations in GL location

Figure S3 - Double-difference interferograms, GL delineations, and bed elevation at Cosgrove and Getz ice shelves

Figure S4 - Indications of seawater intrusions behind the grounding line at Thwaites

Figure S5 - GL delineations and bed elevation at smaller glaciers

Figure S6 - Examples of Sentinel-1 double-difference interferograms with 12-, 6-, and 1-day temporal baselines

S1 - Estimating tide- and pressure-induced sea surface height difference

We estimate changes in sea surface height (SSH) driven by ocean tides using the pyTMD module (Sutterley et al., 2025), which computes tidal elevations based on a given tidal model. Tidal elevations are computed using the CATS2008 model (Howard et al., 2008) for the UTC timestamps of all of the Sentinel-1 acquisitions at the fronts of all major ice shelves located in the Amundsen sector, where grounding lines were mapped. Note that the acquisition times are taken as the sensing time approximately mid-way through the given track - as each track took approximately 2-3 minutes to sense, the SSH variation caused by using a fixed, track-wide acquisition time is negligible. For a given double-difference interferogram, consisting of four images with sensing times (t_1, t_2, t_3, t_4), the expected vertical displacement induced by tidal variation is:

$$\Delta\eta_{DD}^{tide} = (\eta_{t4}^{tide} - \eta_{t3}^{tide}) - (\eta_{t2}^{tide} - \eta_{t1}^{tide}) \tag{S1}$$

where η_t^{tide} is the expected tide elevation at time t, mimicking the double-differencing of the DInSAR phase measurements.

Because SSH is also modulated by atmospheric pressure, known as the inverse barometer effect (IBE), we estimate this component using mean sea level pressure from ERA5 reanalysis data (Hersbach et al., 2023), sampled at an hourly rate. The expected change in SSH, $\Delta\eta^{IBE}$, from a change in pressure, ΔP is (Chelton and Enfield, 1986):

$$\Delta\eta^{IBE} = -\frac{\Delta P}{\rho g} = -\frac{P - P_{ref}}{\rho g} \tag{S2}$$

where $\rho \approx 1025.0$ kg/m^3 and $g \approx 9.81$ m/s^2. The reference pressure, P_{ref}, is usually taken as the long-term mean/median pressure over the region of interest, however, in the double-difference context, P_{ref} cancels out. The expected SSH variation induced by IBE in a double-difference retrieval is:

$$\Delta\eta_{DD}^{IBE} = (\eta_{t4}^{IBE} - \eta_{t3}^{IBE}) - (\eta_{t2}^{IBE} - \eta_{t1}^{IBE}) \tag{S3}$$

The total SSH variation expected for a double-difference retrieval is then simply the combination of the tide and IBE signals:

$$\Delta\eta_{DD}^{total} = \Delta\eta_{DD}^{tide} + \Delta\eta_{DD}^{IBE} \tag{S4}$$

We compute $\Delta\eta_{DD}^{total}$ for each of the 11 generated double-difference interferogram products (Table S1). As mentioned above, we evaluated SSH at a point near the front of each of the major ice shelves (Abbot, Cosgrove, Pine Island, Thwaites, Crosson, Dotson, and Getz). For each double-difference interferogram we computed the average $\Delta\eta_{DD}^{total}$ over all of the points-of-interest and found a relatively modest variation (standard deviation of 2-5 cm). Hence, for simplicity, we provide the mean $\Delta\eta_{DD}^{total}$ in Table S1. As expected, there is good agreement between the estimated $\Delta\eta_{DD}^{total}$ and the observed vertical displacements from the double-difference interferograms (indicated by the amount of fringes at the GL).

We also provide the estimated maximum SSH for each double-difference product, i.e.:

$$\eta_{max}^{total} = \max\left(\eta_{t1}^{total}, \eta_{t2}^{total}, \eta_{t3}^{total}, \eta_{t4}^{total}\right) \tag{S5}$$

as this represents the highest SSH reached during the product's acquisition times, and hence may provide, in some cases, an indication of the expected tide-induced GL migration for the given product.

References

Chelton, D. B. and Enfield, D. B.: Ocean signals in tide gauge records, *J. Geophys. Res.*, 91, 9081–9098, doi:10.1029/JB091iB09p09081, 1986

Hersbach, H., Bell, B., Berrisford, P., Biavati, G., Horányi, A., Muñoz Sabater, J., Nicolas, J., Peubey, C., Radu, R., Rozum, I., Schepers, D., Simmons, A., Soci, C., Dee, D. and Thépaut, J-N.: ERA5 hourly data on single levels from 1940 to present. *Copernicus Climate Change Service (C3S) Climate Data Store (CDS)*, https://doi.org/10.24381/cds.adbb2d47, 2023

Howard, S. L., Erofeeva, S. and Padman, L.: CATS2008: Circum-Antarctic Tidal Simulation version 2008, U.S. Antarctic Program (USAP) Data Center, https://doi.org/10.15784/601235, 2019

Morlighem, M.: MEaSUREs BedMachine Antarctica, Version 3, https://doi.org/10.5067/FPSU0V1MWUB6, 2022

Sutterley, T. C., Howard, S. L., Padman, L. and Siegfried, M.: pyTMD: Python-based tidal prediction software, *Journal of Open Source Software*, 10(116), 8566, https://doi.org/10.21105/joss.08566, 2025

Track	Prod. ID	Acq. 1	Acq. 2	Acq. 3	Acq. 4	$\Delta\eta_{DD}^{total}$	$\Delta\eta_{max}^{total}$	Figure
7	T007_P1	1/17/25 05:08:56	1/18/25 05:07:41	1/29/25 05:08:56	1/30/25 05:07:41	-0.22	1.18	Fig. 2c
7	T007_P2	1/29/25 05:08:56	1/30/25 05:07:41	2/10/25 05:08:55	2/11/25 05:07:41	0.12	1.18	-
7	T007_P3	2/10/25 05:08:55	2/11/25 05:07:41	2/22/25 05:08:55	2/23/25 05:07:41	0.22	1.17	-
7	T007_P4	2/22/25 05:08:55	2/23/25 05:07:41	3/6/25 05:08:55	3/7/25 05:07:41	0.22	1.03	Figs. 2d and S3c
10	T010_P1	1/29/25 10:00:41	1/30/25 09:59:22	2/22/25 10:00:40	2/23/25 09:59:22	0.09	0.78	Fig. S3c
65	T065_P1	1/21/25 04:36:37	1/22/25 04:35:26	2/2/25 04:36:36	2/3/25 04:35:25	-0.27	0.71	Fig. 2b
65	T065_P2	2/2/25 04:36:36	2/3/25 04:35:25	2/14/25 04:36:35	2/15/25 04:35:25	-0.16	0.60	-
65	T065_P3	2/14/25 04:36:35	2/15/25 04:35:25	2/26/25 04:36:35	2/27/25 04:35:25	0.07	0.99	-
68	T068_P1	1/21/25 09:26:54	1/22/25 09:25:36	2/14/25 09:26:53	2/15/25 09:25:35	-0.38	0.64	-
68	T068_P2	1/21/25 09:26:54	1/22/25 09:25:36	2/26/25 09:26:52	2/27/25 09:25:35	-0.01	0.46	Fig. S3a
68	T068_P3	2/14/25 09:26:53	2/15/25 09:25:35	2/26/25 09:26:52	2/27/25 09:25:35	0.38	0.64	Fig. 2a

Table S1. Acquisition times (UTC, format 'day/month/year hour:minute:second') for the generated Sentinel-1 double-difference interferograms along with estimated tide- and IBE-induced sea surface height difference, $\Delta\eta_{DD}^{total}$, and sea surface height maximum, $\Delta\eta_{max}^{total}$, both in units of meters (Section S1). The final column indicates which Figure each double-difference interferogram is displayed in. Dates 1 and 2 indicate the acquisitions used in the first interferogram, while Dates 3 and 4 are the acquisitions from the second interferogram in the double-difference product.

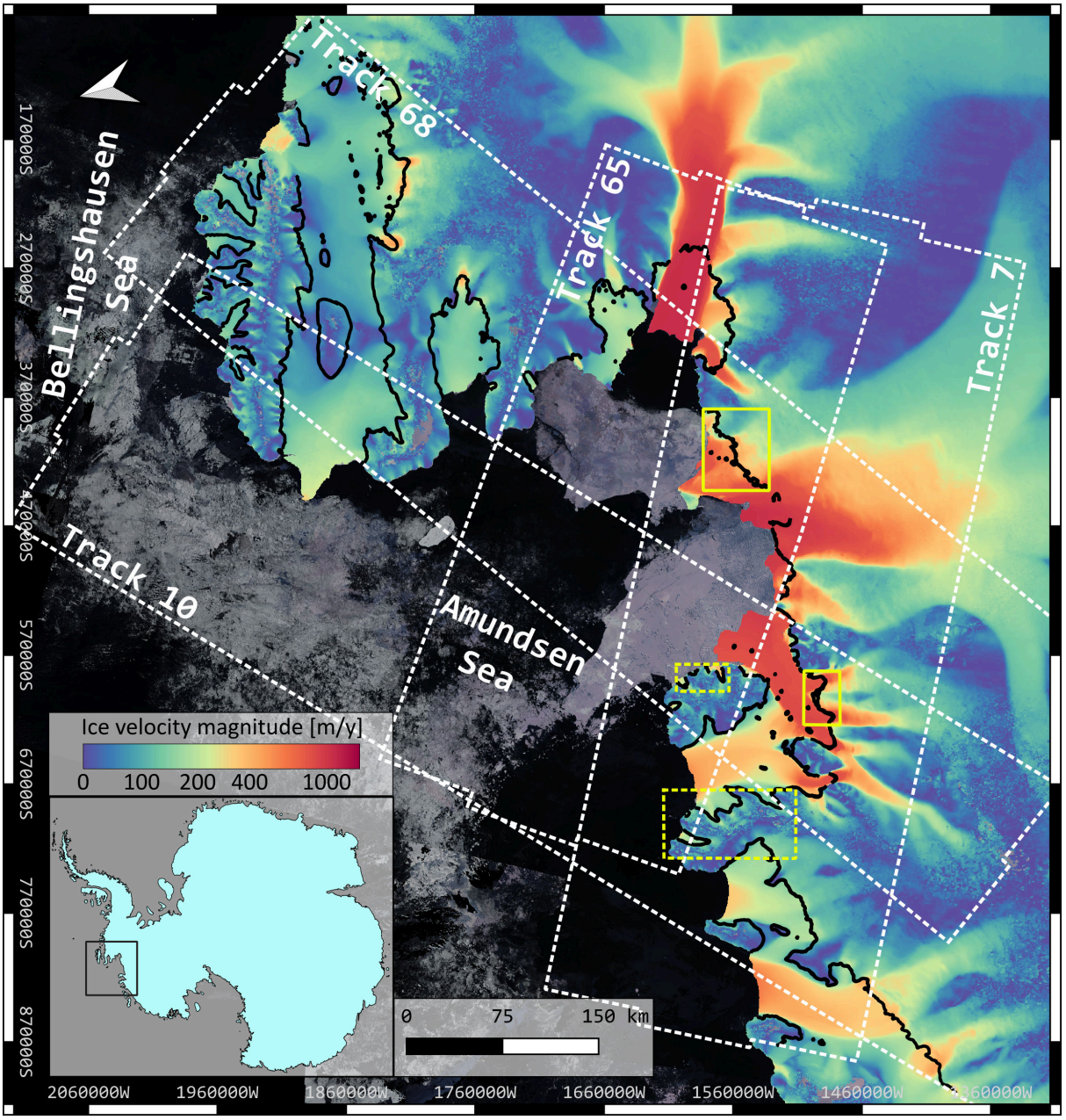

Figure S1. Coverage of the Sentinel-1 1-day repeat-pass data set from January-March 2025 in the Amundsen Sea Embayment. The various tracks (7, 10, 65, 68) are labeled and indicated by white dashed polygons. The 2025 grounding line delineations are indicated by black lines. Solid and dashed yellow rectangles indicate spatial extents in Figures S2 and S5, respectively. The background map shows ice velocity magnitude from MEaSUREs (Rignot et al., 2017), clipped to the 2025 January-March ice shelf extent, overlaid on a Sentinel-2 January-March 2025 true color mosaic. Map projection is EPSG:3031

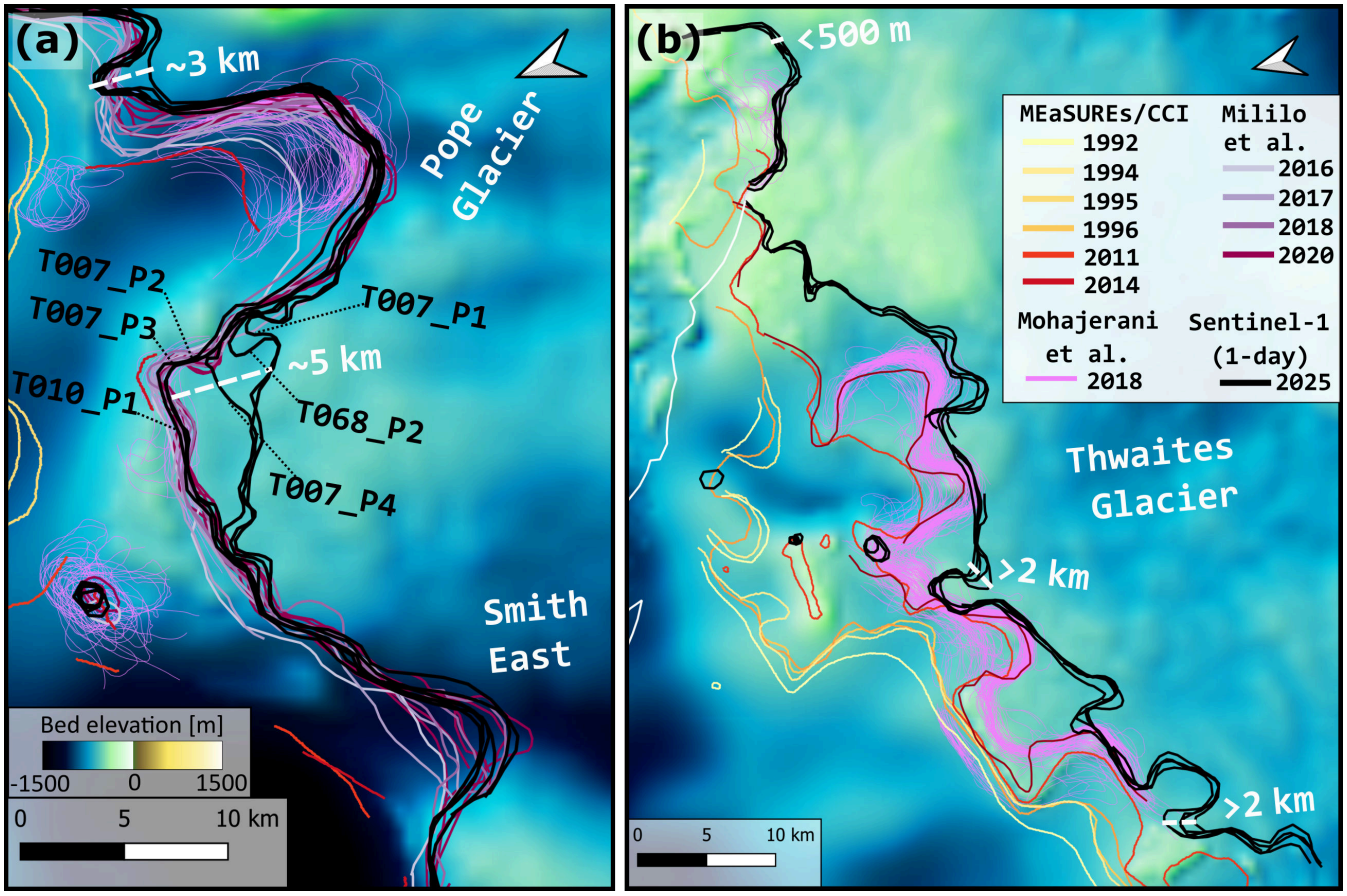

Figure S2. Grounding line locations near Pope and Smith glaciers (a) and the eastern sector of Thwaites glacier (b). Black labels and dashed lines in (a) indicate IDs for the individual 2025 GL delineations (see Table S1). Short-term GL migration of variable magnitude is observed between the various 2025 GLs, spanning less than 500 m to 5 km. While the agreement between $\Delta\eta_{DD}^{total}$ and observed vertical displacement is good, we do not generally observe a consistent correspondence between η_{max}^{total} and GL location.

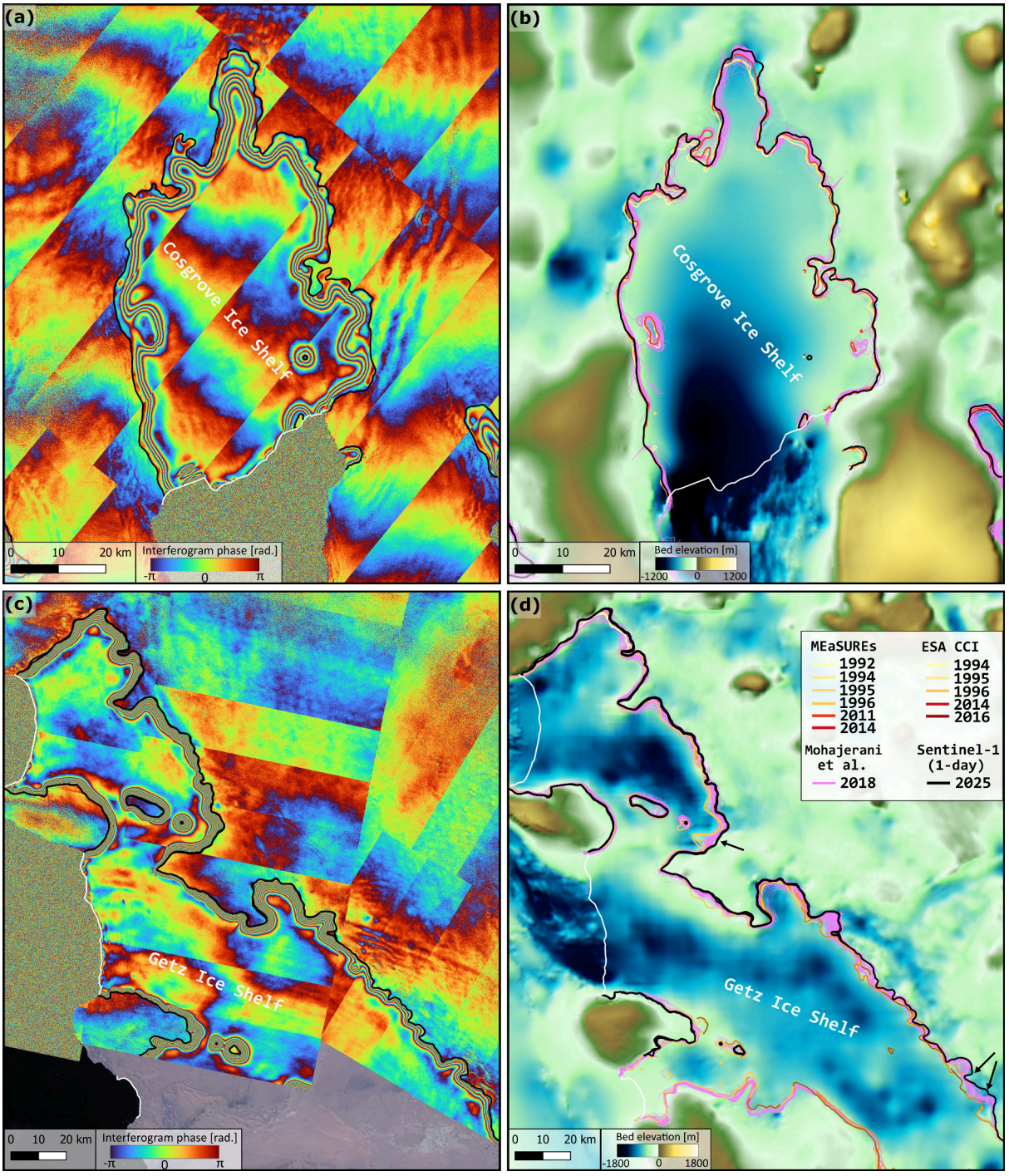

Figure S3. (a) 2025 Sentinel-1 1-day double-difference interferogram, with GL delineations indicated by black lines and (b) bed elevation (Morlighem, 2022) and grounding line delineations (see legend) over Cosgrove Ice Shelf. (c) 2025 Sentinel-1 1-day double-difference interferogram and GL delineations, indicated by black lines and (d) bed elevation and grounding line delineations (see legend) over Getz Ice Shelf. White lines indicate 2025 ice shelf calving front lines. Black arrows in (d) indicate local sectors where the 2025 GL appears $>$ 1 km inland of the 2018 GZ. Acquisition times for the interferograms are provided in Table S1.

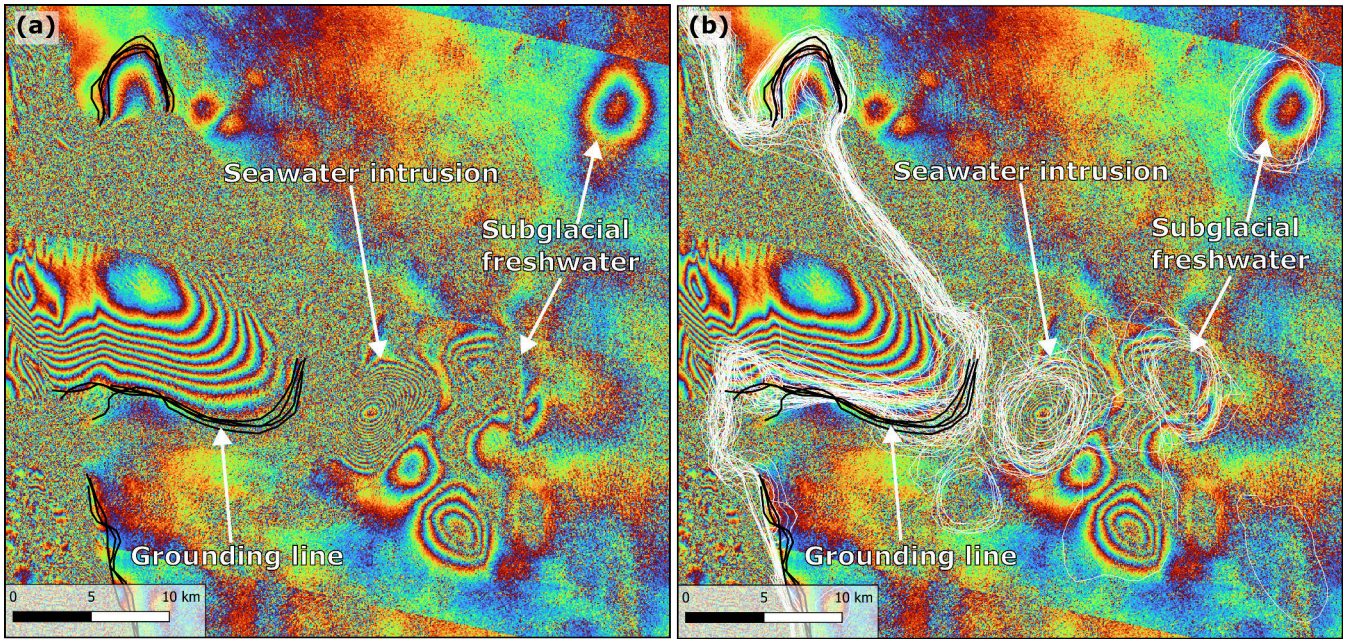

Figure S4. (a) Sentinel-1 double-difference interferogram from Thwaites Glacier (acquisition dates 17th-18th and 29th-30th January 2025, product ID T007_P1) with the updated grounding line delineations indicated by black lines. Apparent seawater intrusion, in the form of a dense circular fringe pattern, is observed behind the typical grounding zone (indicated by a white arrow). At the same time, further inland regions show evidence of propagating subglacial freshwater (causing vertical surface displacements and, hence, fringes in the double-difference interferogram). (b) same as in (a), but with white lines indicating seawater intrusions, subglacial water propagation, and grounding line locations delineated by Rignot et al. (2024) from ICEYE March-June 2023 data.

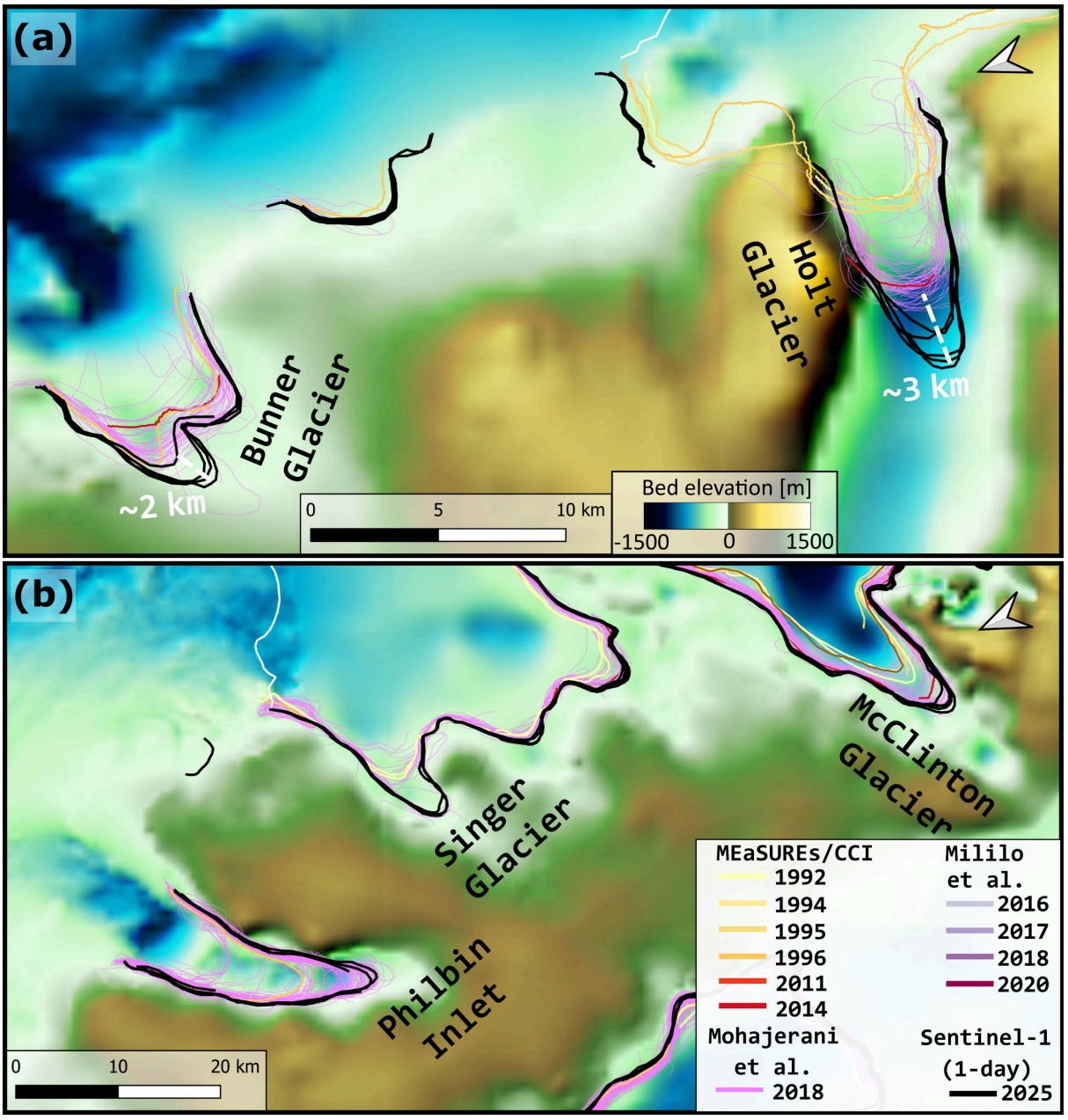

Figure S5. Observed grounding line locations at Bunner and Holt glaciers (a) and Philbin Inlet, Singer, and McClinton glaciers (b). Background map shows bed elevation from Morlighem (2022). All 2025 retrievals lie at or behind the inland limit of the 2018 grounding zone (Mohajerani et al., 2018), suggesting potential retreat of the grounding zone. Holt Glacier appears to have retreated 2-3 km during 2018-2025.

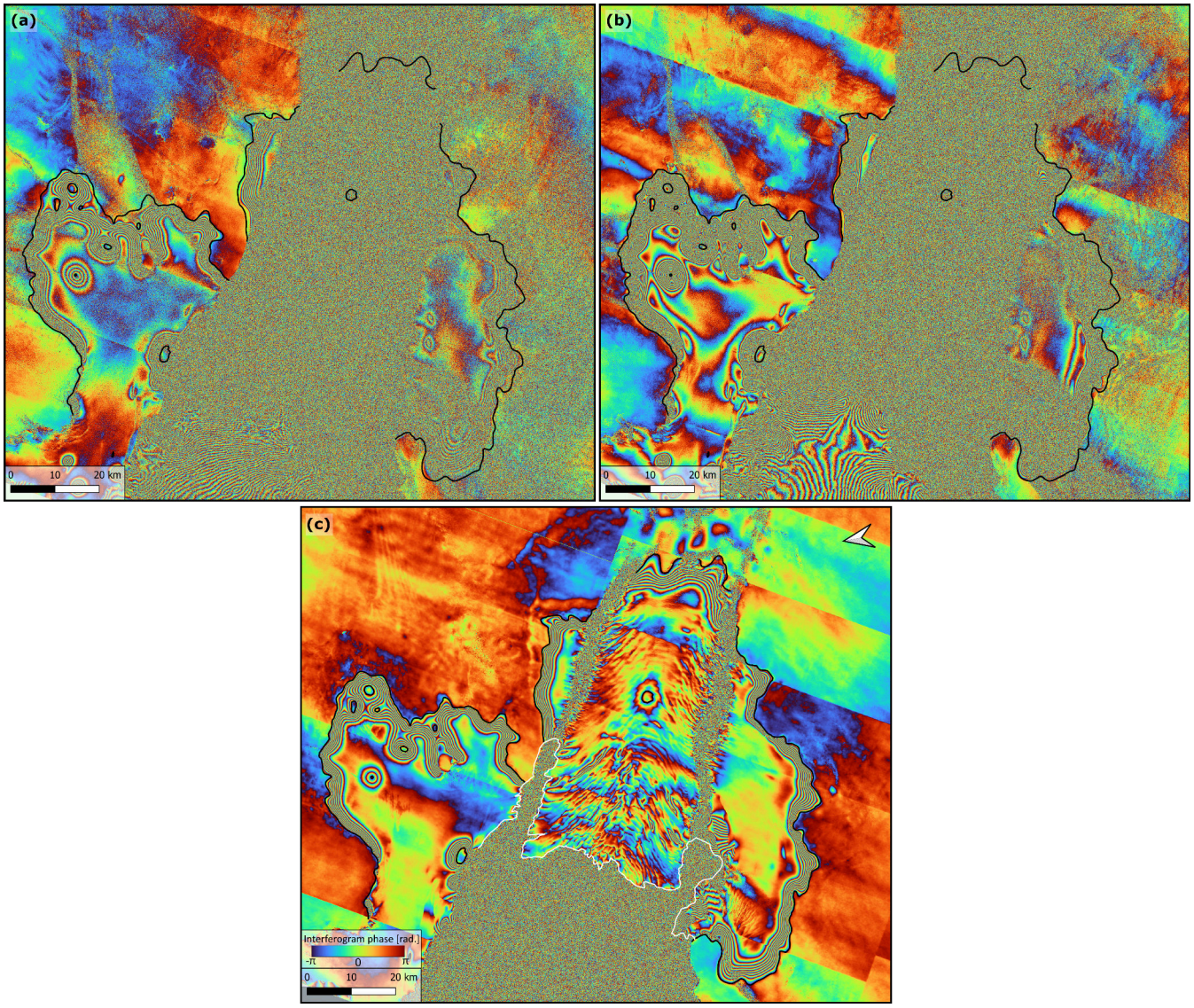

Figure S6. Examples of Sentinel-1 double-difference interferograms from Pine Island Ice Shelf using interferograms with temporal baselines of (a) 12 days, (b) 6 days, and (c) 1 day (same as Figure 2b in the main text). Acquisition dates for panel (a) are 2018/02/15-2018/02/27 and 2018/02/21-2018/03/05, for panel (b) 2018/02/21-2018/02/27 and 2018/02/27-2018/03/05, and for panel (c) 2025/01/21-2025/01/22 and 2025/02/02-2025/02/03 (product ID T065_P1, Table S1). The black lines indicate the 2025 grounding line delineation from the 1-day interferogram (in all panels).